J. Appl. Comput. Mech., 6(2) (2020) 307-319
DOI: 10.22055/JACM.2019.29503.1605

ISSN: 2383-4536
jacm.scu.ac.ir

M&MoCS

Shahid Chamran
University of Ahvaz

Journal of
Applied and Computational Mechanics

Research Paper

Mesoscopic Simulation of Forced Convective Heat Transfer of Carreau-Yasuda Fluid Flow over an Inclined Square: Temperature-dependent Viscosity

A. Jalali[1], A. Amiri Delouei[2], M. Khorashadizadeh[3], A.M. Golmohammadi[4]
S. Karimnejad[5]

[1] Department of Mechanical Engineering, Payame Noor University (PNU), P.O. BOX 19395-3697, Tehran, Iran, Email: a_jalali@pnum.ac.ir
[2] Department of Mechanical Engineering, University of Bojnord, Bojnord, Iran, Email: a.amiri@ub.ac.ir, a.a.delouei@gmail.com
[3] Department of Mechanical Engineering, Payam Noor University, Mashhad, Iran, Email: mojtaba.khorashadi@yahoo.com
[4] Department of Mechanical Engineering, Payam Noor University, Mashhad, Iran, Email: golmohamadi-a@mashhad.ir
[5] Department of Mechanical Engineering, Shahrood University of Technology, Shahrood, Iran, Email: karimnejad.sajjad@gmail.com

Received May 12 2019; Revised June 21 2019; Accepted for publication June 28 2019.
Corresponding authors: Sajjad Karimnejad (karimnejad.sajjad@gmail.com), Amin Amiri Delouei (a.amiri@ub.ac.ir)

Abstract. In the current study, non-Newtonian flow pattern and heat transfer in an enclosure containing a tilted square are examined. In order to numerically simulate the problem, the mesoscopic lattice Boltzmann method is utilized. The non-Newtonian Carreau-Yasuda model is employed. It is able to adequately handle the shear-thinning case. The simulation results of flow and heat transfer have been successfully verified with the previous studies. Several parameters such as Nusselt number, Drag coefficient, and Carreau number are investigated in details. Considering the temperature-dependent viscosity, it is seen that with increasing the temperature-thinning index, the drag coefficient increases, but the Nusselt number decreases. By rotating the square obstacle, the results display that increasing the angle of inclination from zero to 45 degrees, increases both the drag coefficient and the Nusselt number. Also, the highest rate of heat transfer occur at the angle of 45 degrees (diamond); however it has a negative impact on the Drag coefficient.

Keywords: Carreau-Yasuda model, Temperature-dependent viscosity, Inclined square, Lattice Boltzmann method.

1. Introduction

Analyzing the convective heat transfer over a surface is a considerable issue in many technological and environmental processes. Chemical industries, pharmaceutical, surface augmentation using fins, biomass fuels and heat exchangers can be proper examples for this matter [1-7]. Further, the wake dynamics behind obstacles have a tremendous importance which could lead to a complicated fluid flow.

Over the last decades, the lattice Boltzmann method (LBM) has gained great attractions as a substitute to the Navier-Stokes (NS) equations in order to simulate complex fluid flows [8-10]. LBM is a mesoscopic (between microscopic and macroscopic) method. Therefore, instead of tracking the position and velocity of the particles in the system as the molecular dynamics, the fluid domain is described by following the density distribution function. Using explicit LBM a whole lot of significant advantages are achieved including simply employing the boundary conditions to at least first-order accuracy, and contrary to the NS equation, the LBM equation is linear [8, 9]. Particles' distribution function in the

Published online: September 03 2019

LBM evolves from the collision stage and then undergoes the streaming step [8]. Moreover, solving the problems using the lattice Boltzmann equations (LBE) will result in low computational costs along with the opportunity to easily handle the complex outlines [11-13]. The shape of the immersed obstacle makes the computations difficult and realistic, obviously. LBM has been utilized to tackle this issue [15, 16].

Due to the fact that LBM has a kinetic nature, there is no need to solve costly and complex Poisson problems to have stress tensor and pressure field. Also, they are accessible locally [8, 9]. This aspect is important for non-Newtonian fluids which viscosity and shear rate are delicately changing [14]. Non-Newtonian flows as a result of their complicated rheology and shear stress generally have diverse manners. Because of their various applications and usages, the non-Newtonian flows are of great interest [15, 16]. Two frequently-used non-Newtonian fluid models are power-law and Carreau-Yasuda [14, 17]. The power-law model is also advantageous from various viewpoints such as for its simplicity and its versatile behavior [16-18]. There is a reasonably large number of studies using the power-law model [18-22]. Aharonov and Rothman [19] utilized the LBM to tackle the simulation of non-Newtonian fluids for the first time. The power-law model was hired to be used as the fluid. Amiri Delouei et al. [20, 21] used the immersed boundary-lattice Boltzmann method to simulate non-Newtonian fluid flow over a heated cylinder. A technique is developed to calculate the Nusselt number. Moreover, they have studied the freefalling of two identical particles in an enclosure filled with non-Newtonian fluid [18]. The considered non-Newtonian fluid was the power-law model.

Beside the advantages of the power-law model, when it comes to simulating the shear-thinning fluids, which are commonly encountered, it is not suitable. Examples of shear-thinning fluids are polymer solutions, blood, grease and molten. It is shown that heat transfer rate in the case of shear-thinning is more than shear-thickening [23, 24]. Thus, studying and accurately simulating the shear-thinning case will have great outcomes. The Carreau-Yasuda model is capable of showing a wide range of shear-thinning fluids, adequately. The model in comparison with the power-law model which needs three parameters to describe the rheological nature of fluid has five parameters. Studies using the Carreau-Yasuda are rather scarce. LBM has been hired to simulate blood flow (shear-thinning flow) in various researches [25]. Wang and Bernsdorf [26] using the LBM simulated the blood flow by hiring the Carreau-Yasuda model. They have adapted the viscosity to the relaxation time, plus it was locally computed.

Inclusion of heat transfer due to its large occurrences has been the topic of researches [27-30]. In most of which, the viscosity is not related to the temperature and is independent [31-33]. However, in most real cases, the viscosity is strongly dependent on the temperature. Adding this important factor will make the problem even more complicated. Therefore, there is scant literature on this significant issue even in the case of Newtonian fluids. It is known that to obtain real results, the temperature-dependent viscosity must be considered. Amiri Delouei et al. [34] studied the effect of temperature-dependent viscosity for a falling circular particle in a box. Soares et al. [35] studied the forced convection from a circular cylinder. With considering the dependence of viscosity on the temperature, they showed that the rate of heat exchange will be enhanced when viscosity is strongly dependent on the temperature.

The main objective of this paper is to numerically investigate the variations of the viscosity with temperature in the case of non-Newtonian fluid. The shear-thinning case due to its promising results in terms of heat transfer is chosen. While the previous studies are generally limited to the power-law fluid as the non-Newtonian model, here, the Carreau-Yasuda model is hired. In order to make the problem even more practical, an inclined square is used as the obstacle. Several parameters such as Nusselt number, Drag coefficient, and Carreau number have been explored. Moreover, the effect of the obstacle orientation is clarified and the optimum angle of inclination for a better heat transfer is introduced. The rest of the paper is organized as follows. In section 2, the employed non-Newtonian model and lattice Boltzmann approach which has been utilized here are briefly discussed. The grid testing and the code accuracy are checked in section 3. Subsequently, the ongoing problem is noted in section 4 and discussed in details in section 5. Lastly, some conclusions are remarked in section 6.

2. Numerical Formulation

The LBM has been applied to model a variety of fluid flow problems including pulsating flow, simulating blood flow, complex boundaries, turbulence [36], etc. In this section, the numerical method for the non-Newtonian fluid along with the formulation for the temperature-dependent viscosity will be concisely clarified. To study in great details see references [8, 9, 35].

2.1 The non-Newtonian model: Carreau-Yasuda

The Carreau-Yasuda is one of the commonly used models in the case of shear-thinning behavior. The non-Newtonian features of the flow reveals an effective impact of the viscosity (μ) which is considerably related to the shear rate ($\dot{\gamma}$) [35].

$$\mu = k\left|\dot{\gamma}\right|^{n-1} \tag{1}$$

here k is the consistency index of the flow and n refers to the behavior index of the flow which both of them are positive real numbers [16, 17]. If the value of n becomes less than one, the shear-thinning fluid will appear. The shear-thinning (also known as pseudo-plastic) model is of great interest due to its usages in hemodynamical simulations. As discussed earlier, the five-parameter Carreau-Yasuda model in terms of shear-thinning fluids ($0<n\leq1$) such as blood and grease

shows much more tangible physical behaviors. The apparent viscosity is noted as [25];

$$\frac{\mu-\mu_\infty}{\mu_0-\mu_\infty}=[1+(\Gamma\dot{\gamma})^a]^{\frac{n-1}{a}}\ ,\ 0<n\leq 1 \tag{2}$$

where a and Γ are a non-dimensional value and a time constant, in that order. In the case of a=2, Carreau-Yasuda model becomes Carreau model. μ_∞ and μ_0 are the flow viscosity at an infinite shear rate ($\dot{\gamma}\to\infty$) and at zero shear rate ($\dot{\gamma}\to 0$), respectively.

2.2 Lattice Boltzmann method

The LBM which relies on the kinetic theory has been increasingly utilized to treat colloidal systems [1, 9, 11, 37]. In this study, for the incompressible flow, the two-dimensional mesoscopic model (*D2Q9*) in Cartesian coordinate is used (Fig. 1), in which *D* refers to the dimension and *Q* stands for the velocity vectors. In the LBM, the flow is defined via a density distribution function ($f_i\ (x,\ t)$) which allows the fluid to move with speed e_i at time t and space x. i refers to the direction of discrete velocity. The distribution function identifies the possibility of the existence of a volume of flow at a certain place and time.

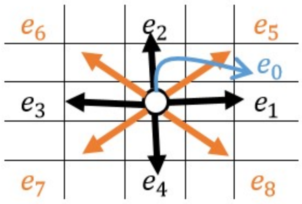

Fig. 1. Velocity directions relating a lattice site to its neighboring positions on a *D2Q9* model

Generally, LBE with single relaxation time (SRT) is adopted in LBM. SRT is initially developed from lattice gas automata [8], it also can be derived from Boltzmann equatuions [5-7]. Owing to SRT's simplicity, it is frequently hired to tackle various problems [15, 16]. The SRT lattice Boltzmann equation is a particular finite difference form of the Boltzmann BGK approximation. It is known as BGK model and the notation is as [8, 9, 11]:

$$f_i(x+e_i\Delta t,t+\Delta t)-f_i(x,t)=-\frac{1}{\lambda_h}[f_i(x,t)-f_i^e(x,t)],\quad (i=0,1,...,8) \tag{3}$$

where f_i and $f_i^{(eq)}$ are density distribution and the equilibrium density distribution function at time "t" and space "x" in the i^{th} discrete velocity direction, correspondingly. Δt and e_i are the time step and lattice speed, respectively. The right-hand side of the Eq. (3) collision term.

$$f_i^e q(x,t)=\omega_i\rho(x,t)[1+\frac{1}{(c_s^2)}(e_i.u(x,t))+\frac{1}{(2c_s^4)}(e_i.u(x,t))^2-\frac{1}{(2c_s^2)}(u(x,t).u(x,t))] \tag{4}$$

λ_h is the dimensionless relaxation time which is related to the kinematic viscosity (v). The relaxation time will help the situation to relax towards the equilibrium state. It must be noted that due to the non-Newtonian nature of the problem, the relaxation time is gotten locally from the distribution functions at each time step. By this mean, we are able to capture the changes in viscosity as a result of shear rate [29, 30]. And from the Chapman-Enskog relation it can be noted as [5-7];

$$\lambda(x,t)=3v(x,t)+\frac{1}{2} \tag{5}$$

$u(x,t)$ and c_s are the lattice speed and the lattice speed of sound which is define by

$$c_s=\frac{e}{\sqrt{3}} \tag{6}$$

ω_i is weighting factor in the i^{th} direction in the case of D2Q9 which are given as [1, 11, 37];

$$\begin{cases}\omega_i=\dfrac{4}{9} & i=0\\ \omega_i=\dfrac{1}{9} & i=1,2,3,4\\ \omega_i=\dfrac{1}{36} & i=5,6,7,8\end{cases} \tag{7}$$

and discrete velocities ($\vec{e}_i$) are specified as follows [8, 11];

$$\vec{e}_i = \begin{cases} 0, & i=0 \\ c\left(\cos\left[\frac{(i-1)\pi}{2}\right], \sin\left[\frac{(i-1)\pi}{2}\right]\right), & i=1,2,3,4 \\ \sqrt{2}c\left(\cos\left[\frac{(i-1)\pi}{2}+\frac{\pi}{4}\right], \sin\left[\frac{(i-1)\pi}{2}+\frac{\pi}{4}\right]\right), & i=5,6,7,8 \end{cases} \tag{8}$$

In which ρ is the fluid density and will be calculated using [8, 11, 14, 37, 38];

$$\rho(x,t) = \sum_{i=0}^{8} f_i(x,t) \tag{9}$$

Finally, the velocity is directly determined using $f_i(x,t)$ as follows [4, 8, 11, 37];

$$\mathrm{u}(x,t) = \frac{1}{\rho(x,t)} \sum_{i=0}^{8} e_i f_i(x,t) \tag{10}$$

2.3 Thermal lattice Boltzmann with temperature-dependent viscosity

The temperature field is utilized in a similar way to the flow domain with its related relaxation time λ_h. For this purpose, a different distribution function is in need, in which it is related to the flow distribution function by getting the macroscopic information (density, velocity) [21].

$$g_i(x+e_i\Delta t, t+\Delta t) - g_i(x,t) = -\frac{1}{\lambda_h}[g_i(x,t) - g_i^e(x,t)], \qquad (i=0,1,\ldots,8) \tag{11}$$

g_i is the distribution function. g_i^{eq} would be the equilibrium distribution function in the direction of i [21];

$$g_i^{eq}(x,t) = \omega_i T(x,t)(1+\frac{3}{c^2}e_i.u(x,t)) \tag{12}$$

ω_i are as the previous form for fluid. Fluid temperature $T(x,t)$ is described via;

$$T(x,t) = \sum_{i=0}^{8} e_i g_i(x,t) \tag{13}$$

Like the flow field, the relaxation time with $\sigma(x,t)$ being the diffusion coefficient read as [21];

$$\lambda_h(x,t) = 3\sigma(x,t) + \frac{1}{2} \tag{14}$$

The relaxation time is connected to the dimensionless thermal diffusivity (β) as follows;

$$\beta = \frac{1}{3}(\lambda_h - 0.5) \tag{15}$$

The fluid viscosity with temperature-dependent formulation which has been introduced by Soares et al. [35] is as;

$$\mu = ke^{-bT}\dot{\gamma}^{n-1} \tag{16}$$

where, T is non-dimensional temperature and b is the temperature-thinning index [35], and for higher values of the temperature-thinning index viscosity dependence will enhance. It is worth noting that this expression is the generalized version of power-law viscosity function for temperature dependence.

$$T = \frac{T - T_w}{T_b - T_w} \tag{17}$$

$$b = \frac{E}{RT_w}\frac{T_b - T_w}{T_w}, \quad T_b\text{-}T_w \ll T_w \tag{18}$$

E is the activation energy. Also, w and R refer to wall and molar gas constant value [35].

3. Grid Study and Verification Test

3.1 Mesh sensitivity

To assess the mesh independency, several Cartesian meshes have been considered. Here, four grids are studied. The cases are M1=50×375, M2=100×750, M3=200×1500 and M4=400×3000 for different behavior indexes, *n,* equal to 0.5. The average Nusselt number is used to investigate the grid sensitivity. As in Table 1, with considering the computational costs and accuracy, with going from M3 to M4 the difference in the outcomes changes inconsiderably; however, the computational time enhances greatly. As a result, M3 with 200×1500 lattice units is chosen in this study.

Table 1. The variations of average Nusselt number for various grids with considering *Re*=60, *Pr*=1, *Ca*=0.32, *n*=0.5, *s*=0.5

Mesh size	M1=50×375	M2=100×750	M3=200×1500	M4=400×3000
The Nusselt number	4.2259	4.4363	4.4712	4.4829
Error	-	4.97%	0.78%	0.26%

3.2 Verification Tests

In order to validate the code and study the authenticity of the work, the outcomes will be compared in this section to the published results. To this aim, the non-dimensional length of the wake (L_r/D) is studied with respect to different Reynolds (*Re*) numbers as in Fig. 2. Breuer et al. [39] proposed the following relation to calculate the aforementioned parameter in the range of 5< *Re*<60 ;

$$\frac{L_r}{D} = -0.065 + 0.054\,\mathrm{Re}\ ,\ 5<Re<60 \tag{19}$$

As illustrated Fig. 2, the obtained results match very well with the work of Breuer et al. [39]. As an additional validation, the Newtonian flow past a fixed square with including the heat transfer is done. As in Fig. 3, the results are compared with those of Dhiman et al. [34]. It confirms that solutions of the present study are reliable and could be used to simulate the ongoing problem.

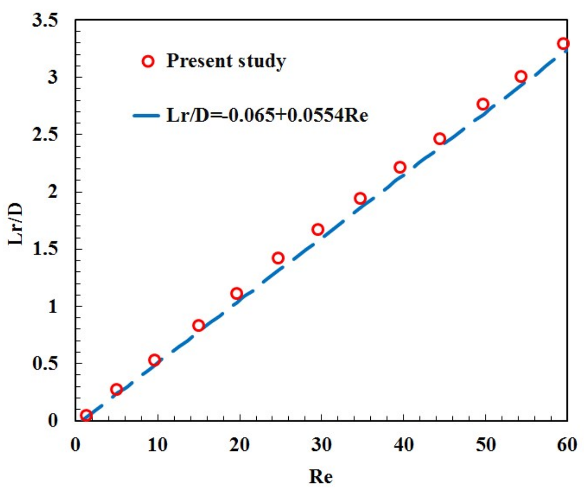

Fig. 2. Wake lengths at various Reynolds numbers L_r/D

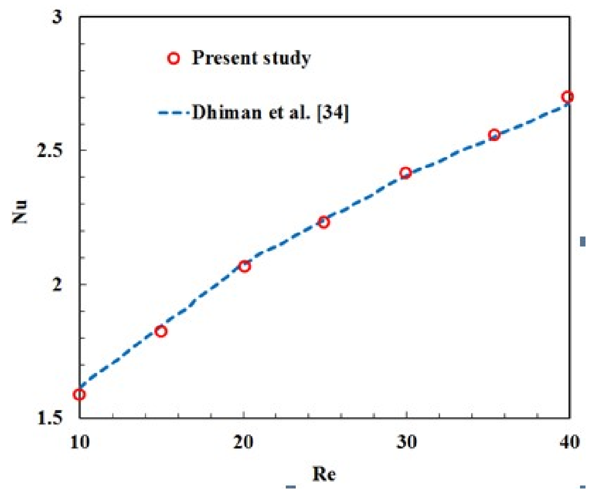

Fig. 3. Nusselt variations at different Reynolds numbers

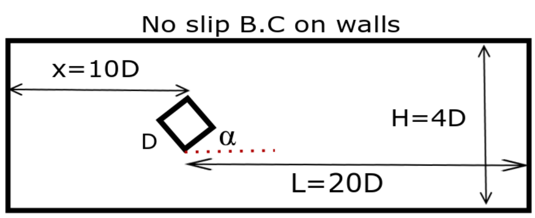

Fig. 4. Schematic illustration of the inclined square in an enclosure

4. Problem Description

The considered configuration is as Fig. 4. As can be seen, the tilted square with side length of *D* is placed in the domain. The no-slip boundary condition is imposed to the boundaries [40]. The method through which boundary treatment is done is the one used in [41] which gives second order accuracy. It is worth mentioning that the method utilized to treat the square is a particular case of it. The square is situated with an initial angle of attack (α). A 200×1500 uniform lattice grid is implemented for the ongoing simulations. The viscosity ratio ($s=\mu_\infty/\mu_0$) equals 0.5 in the simulations unless otherwise stated. For the temperature-thinning index, b, in this study a rather wide range is considered, ($-1<b<1$).

As known, even in the case of Newtonian fluid for the flow past a circular cylinder, the flow regime alters at different Reynolds numbers ($Re = \rho u_0 D / \mu_0$) [35]. Thus, various values of Reynolds numbers are considered in this study ($20< Re <60$). Other non-dimensional numbers are Carreau number (Ca) and Prandtl number (Pr) which are correspondingly noted below;

$$Ca = \frac{\lambda u_0}{D} \tag{20}$$

$$Pr = \frac{\mu_0}{\rho \alpha} \tag{21}$$

In addition, the local Nusselt number (Nu) and average Nusselt number ($\overline{Nu}$) in this study are formulated as;

$$Nu = -\frac{D}{(T_w - T_i)} \left(\frac{\partial T}{\partial n} \right)_{wall} \tag{22}$$

$$\overline{Nu} = -\frac{1}{2\pi} \int_{-\pi}^{\pi} Nu d\theta \tag{23}$$

5. Results and Discussion

In this section, a thermal flow around an isothermal inclined square cylinder is considered. Various parameters are studied in detail and the effect of temperature dependent viscosity is involved. Table 2 gives the length of wakes at different behavior indexes with respect to the Re number. It is seen that the wake length decreases as the n increases at different Re numbers. Moreover, with furthering the thinning behavior of the fluid the separation region will enhance. The variations of drag coefficient (Cd) versus various values of n at three different Reynolds numbers are illustrated in Fig. 5. It is shown that, the drag coefficient with a rise in Re number will be decreased, considerably. It can be found out that regardless of Re number, Cd gradually increases as the index n increases.

Table 2. The wake lengths at Ca=0.32, a=2, s=0.5

Re	n=0.25	n=0.5	n=0.75	n=1
20	0.99	0.979	0.967	0.954
40	1.788	1.756	1.725	1.704
60	2.439	2.381	2.331	2.287

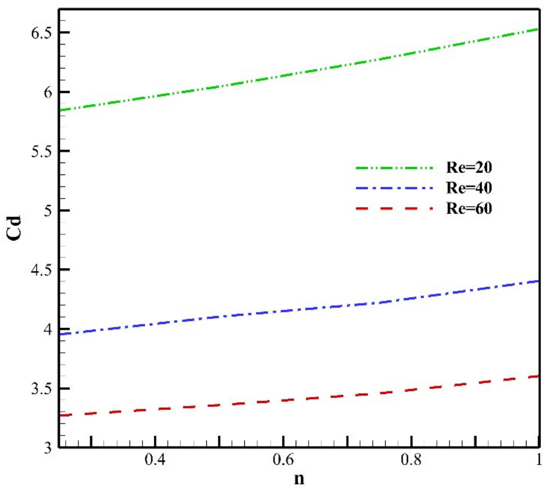

Fig. 5. Variations of drag coefficient with respect to Re and n for Ca=0.32, a=2, s=0.5

Figure 6 illustrates the streamline changes related to three considered Reynolds numbers when n equals one. The angle of orientation is considered zero. It successfully presented the wake behind the obstacle. It is seen that the volume and length of the wake strongly depend on the Re number and the bigger Re is, the larger and longer wake will be. The simulation satisfies the physical situation and sounds reasonable. Figure 7 demonstrates the variations of average Nusselt number against n at different Reynolds numbers. As expected, as Re increases, the average Nusselt number increases and this is due to the growth in the convection heat transfer. Furthermore, the average Nusselt number regardless of Re number decreases as the n increases. One may deduce that the Nu depends on the Re and at higher Re, higher dependence can be seen. In Fig. 8 the temperature field around the obstacle is depicted at different Reynolds numbers. In upper Reynolds numbers the number of isothermals around the obstacle will be augmented, thus the temperature gradient will enhance and as a result, there is a better heat transfer and higher Nusselt number.

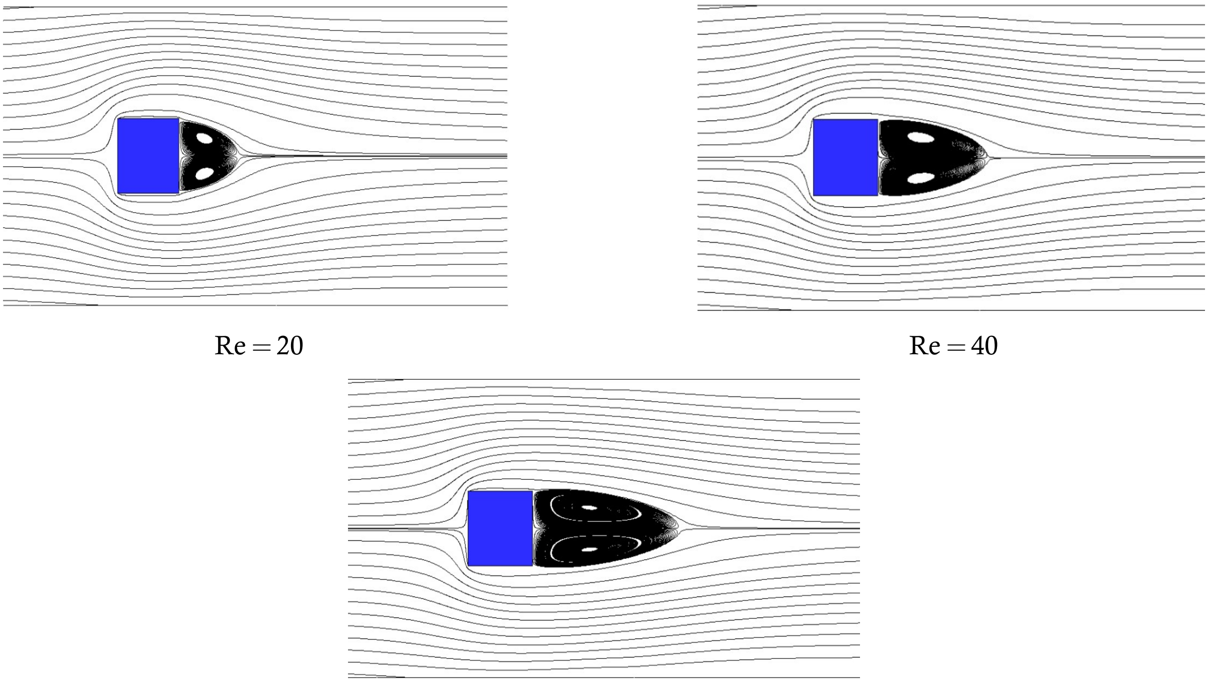

Fig. 6. Contours of streamlines around the square at different Reynolds numbers (n=1)

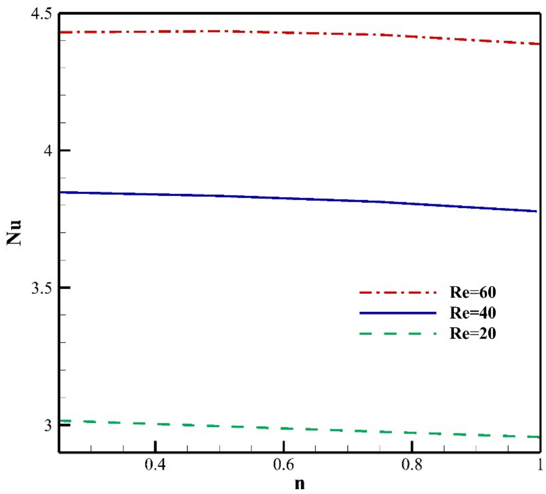

Fig. 7. The average Nusselt number against the flow indices (n) at Ca=0.32, Pr=1 and s=0.5

The trend of Drag coefficient (Cd) with respect to the Carreau number (Ca) at different Reynolds numbers is plotted in Fig. 9. It is known that Ca results in less Cd and it is as a result of shear-thinning occurrence. When the Ca growths the shear-thinning behavior of the fluid appears sooner. As can be seen in Fig. 9, at various Reynolds numbers, Cd lowers as Ca develops. Table 3 presents the variations of Nusselt number at different Carreau numbers. As mentioned earlier, the Carreau number has a part in fluid's behavior (shear-thinning effect). It is worth mentioning that this part is rather small. Changes in Carreau number hardly alter the flow and temperature field. As in Table 3, at different Reynolds numbers, different Carreau numbers change the average Nusselt number.

For an obstacle with square outline, the trend of Drag coefficient against the temperature-thinning index (b) is illustrated in Fig. 10. It underlines the impact of temperature-dependent viscosity. It is seen that the Drag coefficient strongly depends on this factor and as the temperature-thinning index growth the Drag coefficient also enhances. The effects of temperature-thinning index (b) on the Nusselt number are demonstrated in Fig. 11. It is revealed that the temperature-thinning index has a negative impact on the Nusselt number as seen. With increasing b the apparent viscosity grows. Consequently, the hydrodynamic and thermal boundary layer enhances, so the temperature gradient on the cylinder drops which make the Nusselt number less.

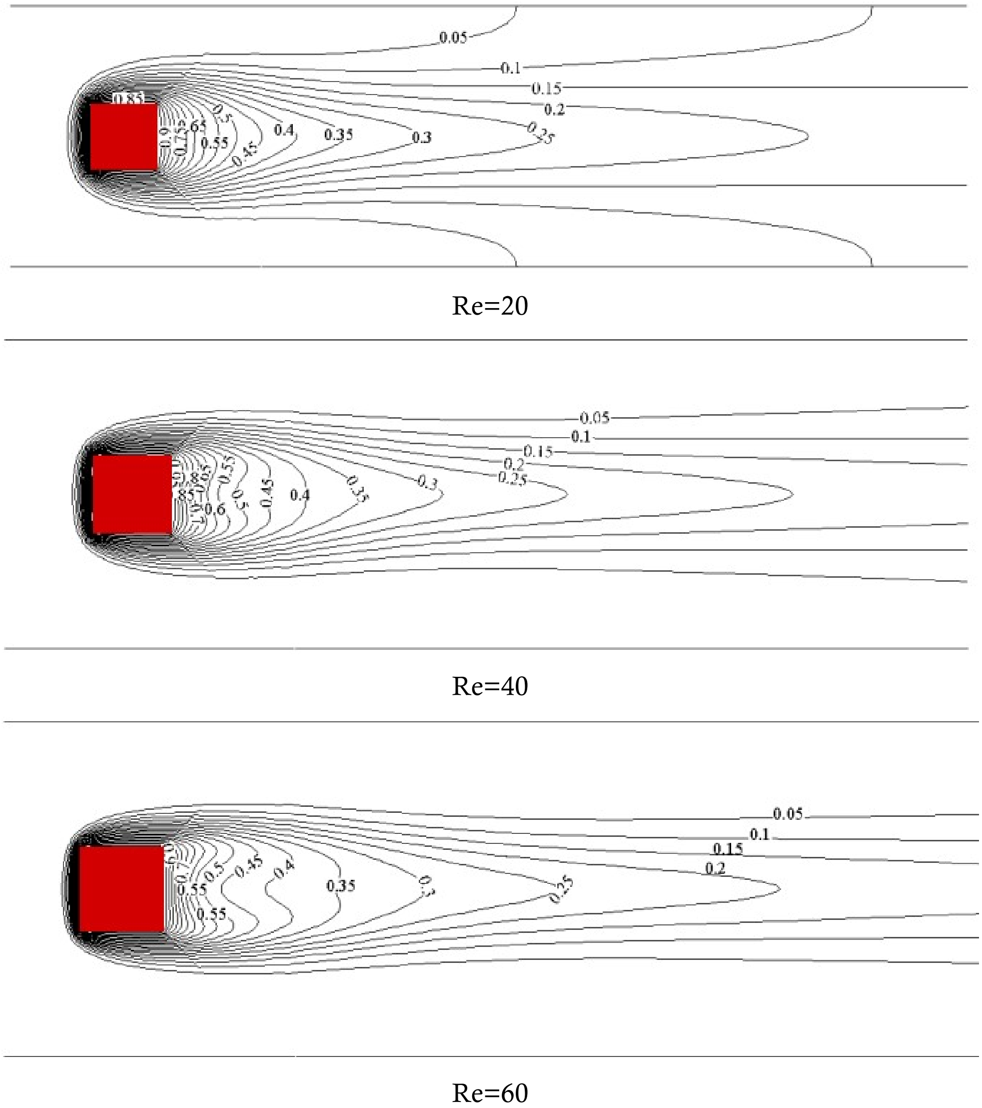

Fig. 8. Isothermal contours around the obstacle at different Reynolds numbers (n=0.5)

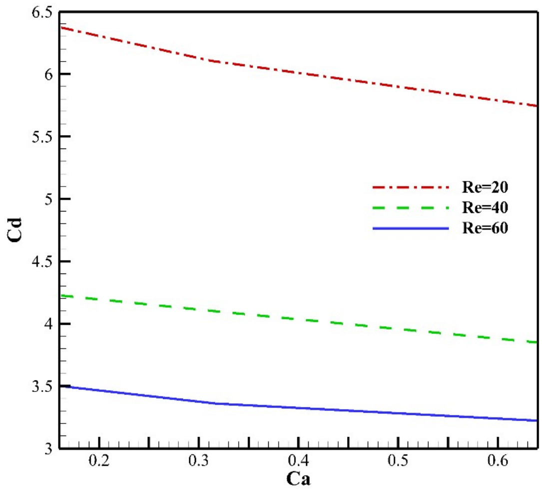

Fig. 9. Drag coefficient against the Carreau number at n=0.5, s=0.5, and a=2

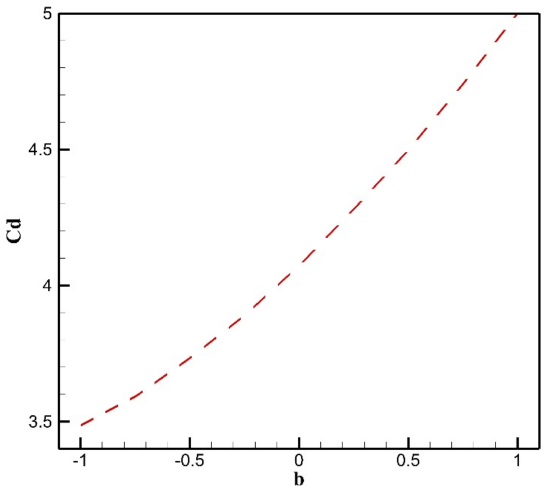

Fig. 10. Variations of Drag coefficient with respect to temperature-thinning index (b) at Ca=0.32, a=2, s=0.5, n=0.5, and Re=40

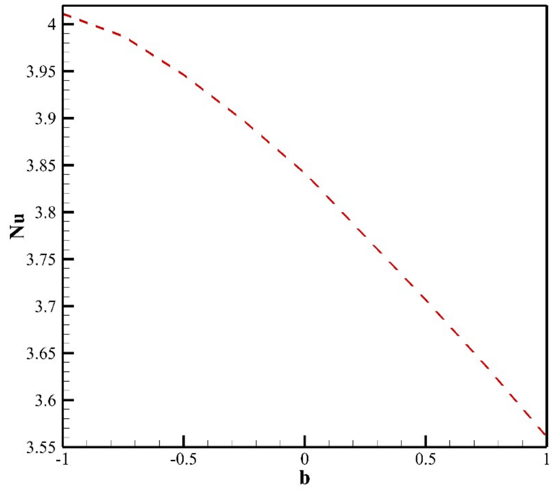

Fig. 11. Variations of Nusselt number against the temperature-thinning index (b) at Ca=0.32, a=2, s=0.5, n=0.5, and Re=40

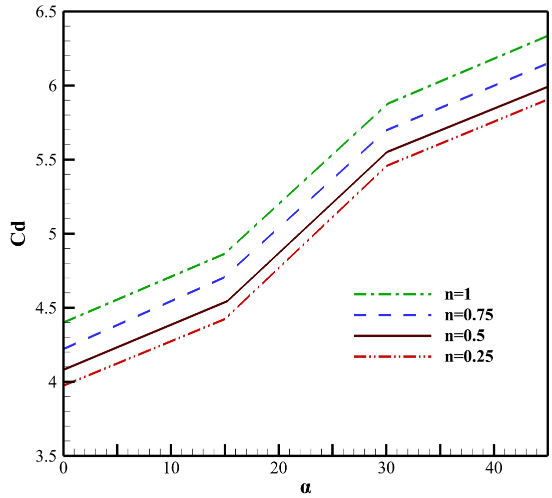

Fig. 12. Effects of n and angle of orientation (α) on the Drag coefficient

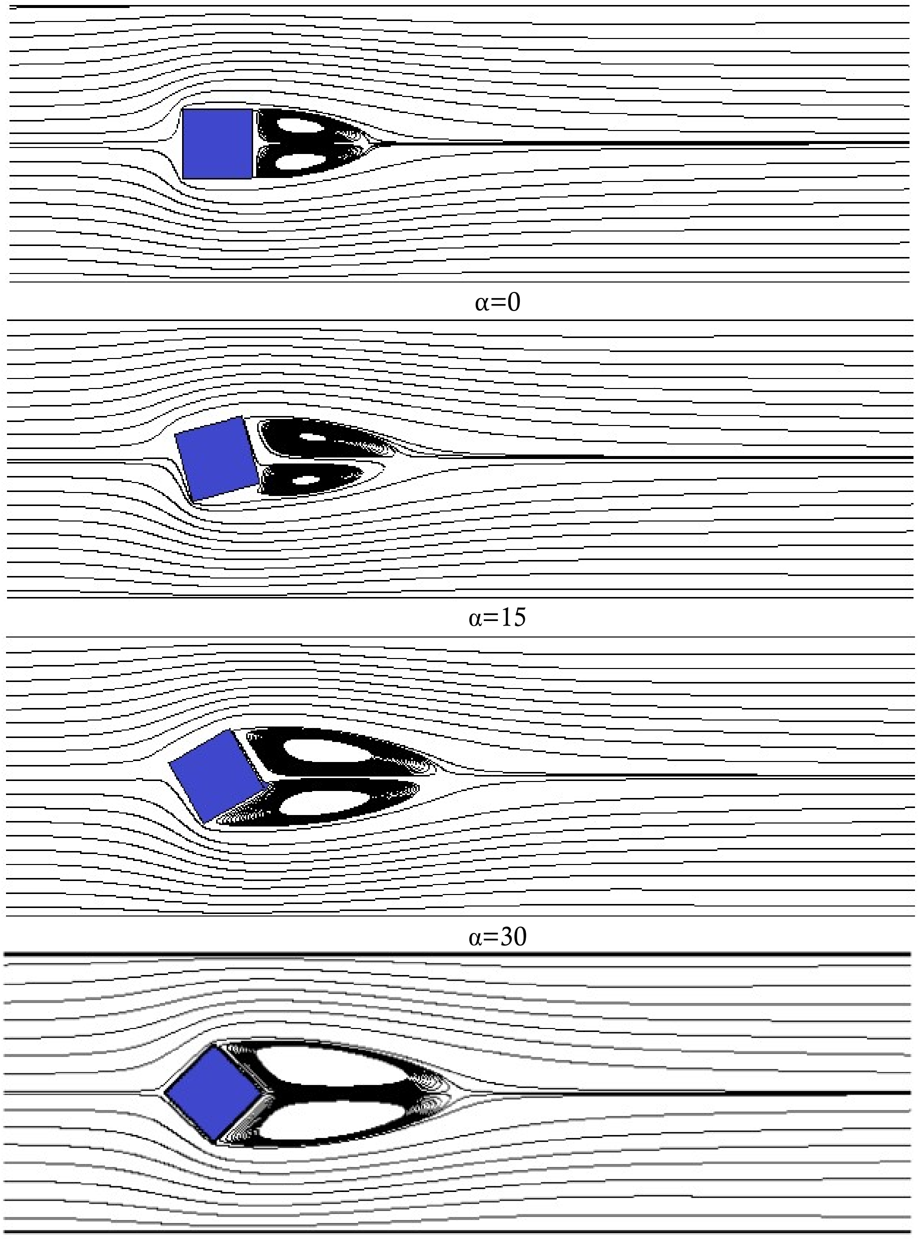

α=0

α=15

α=30

α=45

Fig. 13. Effects of α and Re on the streamlines around the square

In addition, the effect of angle on the heat exchange and flow domain is also investigated. Fig. 12 displays the Drag coefficient at different angle of orientations (α=0, 15, 30, 45). Also, the non-Newtonian index varies. It is seen that with a rise in the angle of orientation (α), the Drag coefficient similarly enhances. This matter at all values of n is seen, and it stems from a large region which flow experiences as the obstacle rotates. Moreover, a weak pressure field will be created behind the obstacle. So, to have the optimum state, the case with zero inclination seems a better choice. The effect of inclination on the streamlines is plotted in Fig. 13. Two wakes are generated as flow passes the obstacle. As mentioned before, when the surface becomes larger, the pressure difference between front and back of the obstacle becomes larger. Consequently, it intensely affects the volume and length of the wakes. At small deviations between 0 to 45 degrees, the wake shape is not symmetric. It is worth mentioning that, with reaching to 45 degree the wakes become balanced and regular once again.

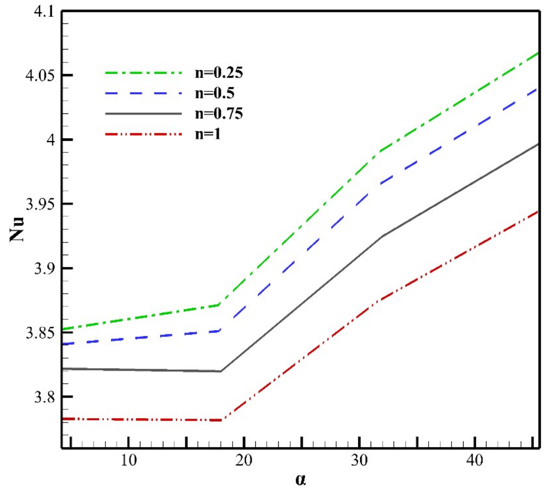

Fig. 14. The variation of the Nusselt number with respect to the α and n at Ca=0.32, s=0.5, a=2, and Re=40

To explore the influence of inclination on the heat exchange, the values of the average Nusselt number at different angle of inclinations are studied (Fig. 14). As for the average Nusselt number, the dependence on the angle is obvious, and it has a positive outcome in terms of heat transfer. Besides, for the Shear-thinning case, as the shear-thinning behavior growth, the heat transfer rises, as anticipated. It is fair to conclude that the rate of heat transfer is high with the obstacle being at α=45 which is because of the large surface area.

Representative plots of isothermal contours in Fig. 15 reveal that isothermal symmetry breaks as the obstacle rotates until α=45. It can be found out that with a growth in α, an agglomeration of isothermals will be generated, thus it directly shakes the Nusselt number and heat exchange.

Table 3. The average Nusselt number with respect to the different Carreau numbers for s=0.5, a=2, n=0.5

Re	Ca=0.16	Ca=0.32	Ca=0.64
20	2.9869	3.0004	3.0082
40	3.8331	3.8418	3.8413
60	4.4388	4.4363	4.4227

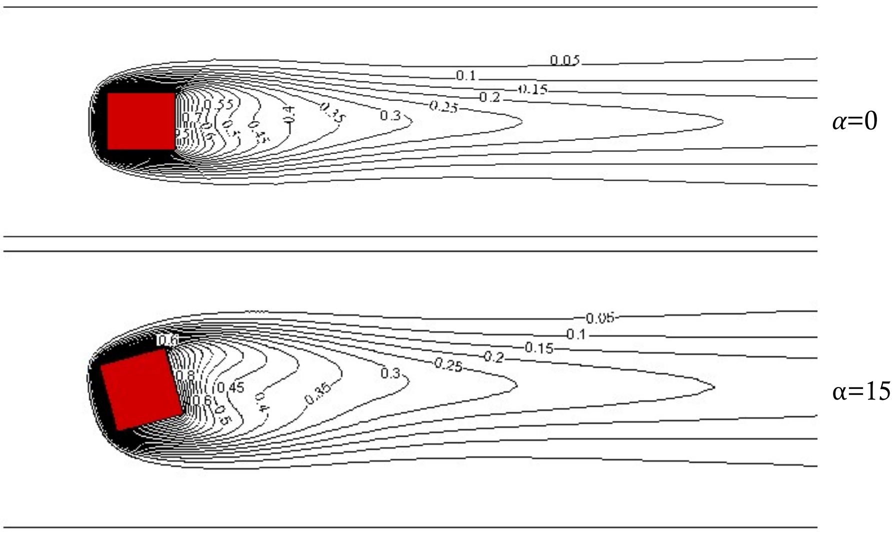

Fig. 15. Isothermals around the tilted square at Re=40 and n=1

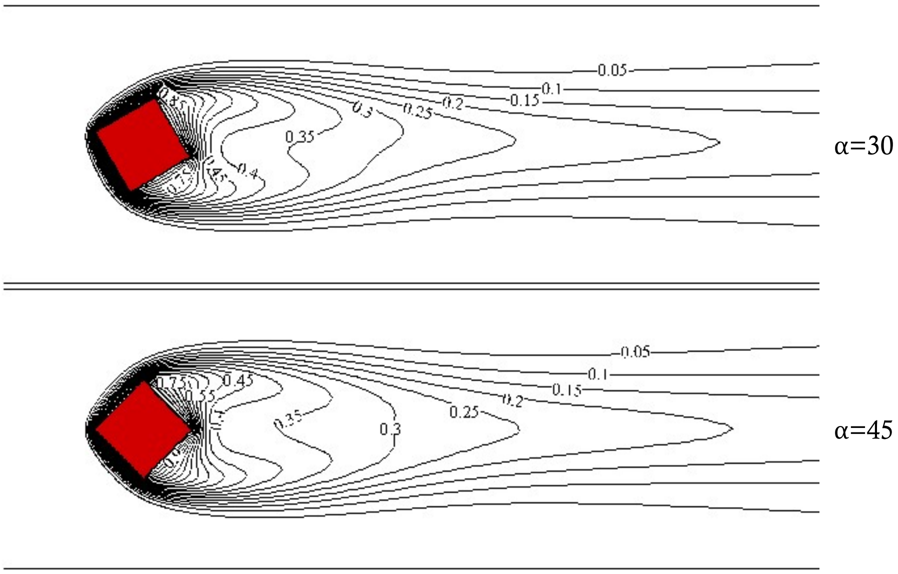

Fig. 15. Continued.

6. Conclusion

The mesoscopic LBM is employed to simulate and assess the heat transfer and flow patterns of a non-Newtonian fluid flow over an inclined square in the case of temperature-dependent viscosity. A wide range of temperature-thinning indices ($-1<b<1$) is considered. Shear-thinning state is considered due to its high rate of heat exchange. As a substitute to the frequently used power-law model, Carreau-Yasuda model is used to be responsible for the non-Newtonian model. The effect of a non-circularity and in particular, square, is involved. Separate validation tests for flow and heat transfer are done to check the code accuracy. Several parameters such as Nusselt number, Drag coefficient, and Carreau number have been included in the simulations and the effects are illustrated. It is displayed that temperature-thinning index has a negative impact on the Drag coefficient. The special case of the tilted square is assessed to study flow and the rate of heat transfer at altered angles (α=0, 15, 30, 45). The results suggest that as the angle of inclination increases, the values of Drag coefficient and Nusselt number enhance. It is concluded that the optimum angle for a better rate of heat transfer would be the last case (α=45) with diamond shape. The outcomes of this study offer an interesting insight for understanding the effect of non-circularity along with a realistic simulation of flow and heat transfer due to the involvement of temperature-dependent viscosity and angle of orientation, simultaneously.

Conflict of Interest

The authors declared no potential conflicts of interest with respect to the research, authorship and publication of this article.

Funding

The authors received no financial support for the research, authorship and publication of this article.

Nomenclature

a	Non-dimensional value	Nu	Nusselt number
b	Temperature-thinning index	Pr	Prandtl number
Ca	Carreau number	s	Viscosity ratio
Cd	Drag coefficient	t	Time
c_s	Speed of sound	T	Temperature
D	Side length of square	$\vec{u}$	Velocity
$\vec{e}_i$	Velocity vector of the lattice	w	Wall
E	Activation energy	***Greek symbols***	
f_i	Particle density distribution function	α	Angle of orientation
$f_i^{(eq)}$	Equilibrium distribution function	β	Thermal diffusivity
F_i	Discrete external force function	ν	Kinematic viscosity
F_{tot}	Total force acting on the particle	ρ	Density
g_i	Internal energy density distribution function	μ	Viscosity

$g_i^{(eq)}$	Equilibrium Internal energy density Distribution function	λ	Single relaxation time
R	Molar gas constant	ω	Weighting factor
Re	Reynolds number	σ	Thermal relaxation time
L_r	Wake lenght	Ω	Collision operator
i	Direction	$\dot{\gamma}$	Shear rate
n	Non-Newtonian behavior index	Γ	n-dimensional value

References

[1] M. Izadi, R. Mohebbi, H. Sajjadi, and A. A. Delouei, LTNE modeling of Magneto-Ferro natural convection inside a porous enclosure exposed to nonuniform magnetic field, *Physica A: Statistical Mechanics and its Applications*, 535, 2019, 122394.

[2] M. Bhatti, A. Zeeshan, and N. Ijaz, Slip effects and endoscopy analysis on blood flow of particle-fluid suspension induced by peristaltic wave, *Journal of Molecular Liquids,* 218, 2016, 240-245.

[3] P. Mellin, E. Kantarelis, and W. Yang, Computational fluid dynamics modeling of biomass fast pyrolysis in a fluidized bed reactor, using a comprehensive chemistry scheme, *Fuel,* 117, 2014, 704-715.

[4] H. Huang, K. Wang, and H. Zhao, Numerical study of pressure drop and diffusional collection efficiency of several typical noncircular fibers in filtration, *Powder Technology,* 292, 2016, 232-241.

[5] M. A. Dandan, S. Samion, M. N. Musa, and F. M. Zawawi, Evaluation of Lift and Drag Force of Outward Dimple Cylinder Using Wind Tunnel, *CFD Letters*, 11(3), 2019, 145-153.

[6] A. A. R. Alkumait, M. H. Zaidan, and T. K. Ibrahim, Numerical Investigation of Forced Convection Flow over Backward Facing Step Affected By A Baffle Position, *Journal of Advanced Research in Fluid Mechanics and Thermal Sciences,* 52(1), 2018, 33-45.

[7] K. Prasad, H. Vaidya, K. Vajravelu, and U. Vishwanatha, Influence of Variable Liquid Properties on Mixed Convective MHD Flow over a Slippery Slender Elastic Sheet with Convective Boundary Condition, *Journal of Advanced Research in Fluid Mechanics and Thermal Sciences*, 56(1), 2019, 100-123.

[8] S. Succi, *The lattice Boltzmann equation: for fluid dynamics and beyond*. Oxford university press, 2001.

[9] C. K. Aidun and J. R. Clausen, Lattice-Boltzmann method for complex flows, *Annual Review of Fluid Mechanics,* 42, 2010, 439-472.

[10] H. Xu, Z. Xing, and K. Vafai, Analytical considerations of flow/thermal coupling of nanofluids in foam metals with local thermal non-equilibrium (LTNE) phenomena and inhomogeneous nanoparticle distribution, *International Journal of Heat and Fluid Flow,* 77, 2019, 242-255.

[11] A. Mohamad, *Lattice Boltzmann Method*. Springer, 2011.

[12] S. Ubertini and S. Succi, Recent advances of lattice Boltzmann techniques on unstructured grids, *Progress in Computational Fluid Dynamics, an International Journal,* 5(1-2), 2004, 85-96.

[13] H. Xu and Z. Xing, The lattice Boltzmann modeling on the nanofluid natural convective transport in a cavity filled with a porous foam, *International Communications in Heat and Mass Transfer,* 89, 2017, 73-82.

[14] S. Karimnejad, A. A. Delouei, M. Nazari, M. Shahmardan, and A. Mohamad, Sedimentation of elliptical particles using Immersed Boundary–Lattice Boltzmann Method: A complementary repulsive force model, *Journal of Molecular Liquids,* 262, 2018, 180-193.

[15] S. Karimnejad, A. A. Delouei, M. Nazari, M. Shahmardan, M. Rashidi, and S. Wongwises, Immersed boundary—thermal lattice Boltzmann method for the moving simulation of non-isothermal elliptical particles, *Journal of Thermal Analysis and Calorimetry,* 2019, DOI: 10.1007/s10973-019-08329-y.

[16] T. N. Phillips and G. W. Roberts, Lattice Boltzmann models for non-Newtonian flows, *IMA Journal of Applied Mathematics,* 76(5), 2011, 790-816.

[17] R. P. Chhabra, *Bubbles, drops, and particles in non-Newtonian fluids*. CRC press, 2006.

[18] A. De Rosis, Harmonic oscillations of laminae in non-Newtonian fluids: a lattice Boltzmann-immersed boundary approach, *Advances in Water Resources,* 73, 2014, 97-107.

[19] A. E. F. Monfared, A. Sarrafi, S. Jafari, and M. Schaffie, Thermal flux simulations by lattice Boltzmann method; investigation of high Richardson number cross flows over tandem square cylinders, *International Journal of Heat and Mass Transfer,* 86, 2015, 563-580.

[20] A. A. Delouei, M. Nazari, M. Kayhani, S. Kang, and S. Succi, Non-Newtonian particulate flow simulation: A direct-forcing immersed boundary–lattice Boltzmann approach, *Physica A: Statistical Mechanics and its Applications,* 447, 2016, 1-20.

[21] E. Aharonov and D. H. Rothman, Non-Newtonian flow (through porous media): A lattice-Boltzmann method, *Geophysical Research Letters,* 20(8), 1993, 679-682.

[22] A. A. Delouei, M. Nazari, M. Kayhani, and S. Succi, Non-Newtonian unconfined flow and heat transfer over a heated cylinder using the direct-forcing immersed boundary–thermal lattice Boltzmann method, *Physical Review E,* 89(5), 2014, 053312.

[23] A. A. Delouei, M. Nazari, M. Kayhani, and S. Succi, Immersed boundary–thermal lattice Boltzmann methods for

non-Newtonian flows over a heated cylinder: a comparative study, *Communications in Computational Physics,* 18(2), 2015, 489-515.
[24] S. Gabbanelli, G. Drazer, and J. Koplik, Lattice Boltzmann method for non-Newtonian (power-law) fluids, *Physical Review E,* 72(4), 2005, 046312.
[25] C. Sasmal and R. Chhabra, Effect of aspect ratio on natural convection in power-law liquids from a heated horizontal elliptic cylinder, *International Journal of Heat and Mass Transfer,* 55(17-18), 2012, 4886-4899.
[26] A. K. Tiwari and R. Chhabra, Laminar natural convection in power-law liquids from a heated semi-circular cylinder with its flat side oriented downward, *International Journal of Heat and Mass Transfer,* 58(1-2), 2013, 553-567.
[27] M. Ashrafizaadeh and H. Bakhshaei, A comparison of non-Newtonian models for lattice Boltzmann blood flow simulations, *Computers & Mathematics with Applications,* 58(5), 2009, 1045-1054.
[28] D. Wang and J. Bernsdorf, Lattice Boltzmann simulation of steady non-Newtonian blood flow in a 3D generic stenosis case, *Computers & Mathematics with Applications,* 58(5), 2009, 1030-1034.
[29] Z.-G. Feng and E. E. Michaelides, Inclusion of heat transfer computations for particle laden flows, *Physics of Fluids,* 20(4), 2008, 040604.
[30] M. Sheikholeslami, H. Ashorynejad, and P. Rana, Lattice Boltzmann simulation of nanofluid heat transfer enhancement and entropy generation, *Journal of Molecular Liquids,* 214, 2016, 86-95.
[31] H. Xu, Z. Xing, F. Wang, and Z. Cheng, Review on heat conduction, heat convection, thermal radiation and phase change heat transfer of nanofluids in porous media: Fundamentals and applications, *Chemical Engineering Science,* 195, 2019, 462-483.
[32] H. Xu, L. Gong, S. Huang, and M. Xu, Flow and heat transfer characteristics of nanofluid flowing through metal foams, *International Journal of Heat and Mass Transfer,* 83, 2015, 399-407.
[33] G. Barrios, R. Rechtman, J. Rojas, and R. Tovar, The lattice Boltzmann equation for natural convection in a two-dimensional cavity with a partially heated wall, *Journal of Fluid Mechanics,* 522, 2005, 91-100.
[34] A. Dhiman, R. Chhabra, and V. Eswaran, Flow and heat transfer across a confined square cylinder in the steady flow regime: effect of Peclet number, *International Journal of Heat and Mass Transfer,* 48(21-22), 2005, 4598-4614.
[35] A. Korichi and L. Oufer, Numerical heat transfer in a rectangular channel with mounted obstacles on upper and lower walls, *International Journal of Thermal Sciences,* 44(7), 2005, 644-655.
[36] A. A. Delouei, M. Nazari, M. Kayhani, and G. Ahmadi, Direct-forcing immersed boundary–non-Newtonian lattice Boltzmann method for transient non-isothermal sedimentation, *Journal of Aerosol Science,* 104, 2017, 106-122.
[37] A. Soares, J. Ferreira, L. Caramelo, J. Anacleto, and R. Chhabra, Effect of temperature-dependent viscosity on forced convection heat transfer from a cylinder in crossflow of power-law fluids, *International Journal of Heat and Mass Transfer,* 53(21-22), 2010, 4728-4740.
[38] R. Mohebbi, M. Izadi, H. Sajjadi, A. A. Delouei, and M. A. Sheremet, Examining of nanofluid natural convection heat transfer in a Γ-shaped enclosure including a rectangular hot obstacle using the lattice Boltzmann method, *Physica A: Statistical Mechanics and its Applications*, 526, 2019, 120831.
[39] M. Breuer, J. Bernsdorf, T. Zeiser, and F. Durst, Accurate computations of the laminar flow past a square cylinder based on two different methods: lattice-Boltzmann and finite-volume, *International Journal of Heat and Fluid Flow,* 21(2), 2000, 186-196.
[40] Q. Zou and X. He, On pressure and velocity boundary conditions for the lattice Boltzmann BGK model, *Physics of Fluids,* 9(6), 1997, 1591-1598.
[41] Mei R., Yu D., Shyy W., and Luo L.-S., Force evaluation in the lattice Boltzmann method involving curved geometry, *Physical Review E*, 65, 2002, 041203.

ORCID iD

Amin Amiri Delouei https://orcid.org/0000-0001-7414-4195
Sajjad Karimnejad https://orcid.org/0000-0002-2691-181X